Oxygen-vacancy and depth-dependent violet double-peak photoluminescence from ultrathin cuboid SnO_2 nanocrystals

L. Z. Liu,[1] X. L. Wu,[1,a)] J. Q. Xu,[1] T. H. Li,[1,2] J. C. Shen,[1] and Paul K. Chu[3,a)]
[1]*National Laboratory of Solid State Microstructures and Department of Physics, Nanjing University, Nanjing 210093, People's Republic of China*
[2]*College of Electronic Engineering, Guangxi Normal University, Guilin 541004, People's Republic of China*
[3]*Department of Physics and Materials Science, City University of Hong Kong, Tat Chee Avenue, Kowloon, Hong Kong, China*

(Received 11 December 2011; accepted 3 March 2012; published online 20 March 2012)

A double peak in the violet region between 360 and 400 nm is observed from the photoluminescence spectra acquired from cuboid SnO_2 nanocrystals and the energy separation between the two subpeaks increases with nanocrystal size. The phenomenon arises from band edge recombination caused by different in-depth distributions of oxygen vacancies (OVs). Density functional theory calculations disclose that variations in the oxygen vacancies with depth introduce valence-band peak splitting leading to the observed splitting and shift of the double peak. © *2012 American Institute of Physics*. [http://dx.doi.org/10.1063/1.3696044]

As an n-type wide band gap semiconductor ($E_g = 3.6$ eV at 300 K), tin oxide (SnO_2) has many potential applications in biophysics, gas sensing, catalysis, and batteries.[1–5] However, despite a large exciton binding energy of 130 meV, development of optoelectronic devices encompassing bulk SnO_2 materials has been hampered by its dipole forbidden nature.[6,7] Fortunately, changes in the symmetry of the nanostructures induced by surface states may allow direct gap transitions[8,9] rendering quantum-confined photoluminescence (PL) possible.[10,11] The surface of a metal oxide nanostructure plays a crucial role in the PL characteristics which can be modified by the addition of oxygen vacancies (OVs), especially nanostructures with small size. Although the PL peaks are typically attributed to radiative recombination in some defect states such as tin interstitials, dangling bonds, or OVs, rigorous confirmation has not been performed.[12,13] Theoretical derivations disclose that the highest occupied orbitals are localized at the surface OVs, thus giving rise to many new energy states in the band gap.[14] Hence, the optical properties are related to the complicated optical transition induced by OVs. It is well known that OVs exist at different depths in metal oxides and so a better understanding of their role and effects is of scientific and practical interest. Cuboid nanocrystals (NCs) have a large surface-to-volume ratio and so surface atoms and electronic states play a key role in the luminescence behavior. In this work, the effects of the different OV distributions with depth in cuboid SnO_2 NCs on the PL behavior are investigated. The double peak appears in the violet range and the separation between the two subpeaks increases with cuboid NC length. In addition to experimental investigation, theoretical derivation based on the density functional theory (DFT) is performed to elucidate the mechanism.

SnO_2 NC samples were prepared using a hydrothermal reaction involving $SnCl_4 \cdot 5H_2O$ and $CO(NH_2)_2$. In a typical process, 0.08 g of $SnCl_4 \cdot 5H_2O$ and 0.8 g of $CO(NH_2)_2$ were added to a 40 ml cylindrical teflon-lined stainless steel autoclave containing 32 ml of deionized water, and 1.6 ml of HCl fume was introduced, followed by ultrasonic treatment and heating to 90 °C for 15 h. After the reaction, the autoclave was cooled to room temperature naturally. The white precipitates were centrifuged and rinsed thoroughly with water several times. The SnO_2 NC colloidal suspensions were used in the experiments and the partial colloidal suspensions were oven-dried in air at 100 °C for 5 h. The samples were characterized by high-resolution transmission electron microscopy (HR-TEM, JEOL-2100), Raman scattering, PL excitation, and x-ray photoelectron spectroscopy (XPS).[15,16] All the measurements were conducted at room temperature.

The PL spectra acquired from the colloidal suspension containing SnO_2 NCs with different sizes excited by the 280–310 nm lines of a Xe lamp are shown in Fig. 1(a). As the average NC size increases (that is, with increasing excitation wavelength from 280–310 nm), a double peak emerges from the PL spectrum. The high energy subpeak (S_1) position [~356 nm (3.48 eV)] does not vary, but the low energy subpeak (S_2) downshifts to ~397 nm (3.12 eV) with

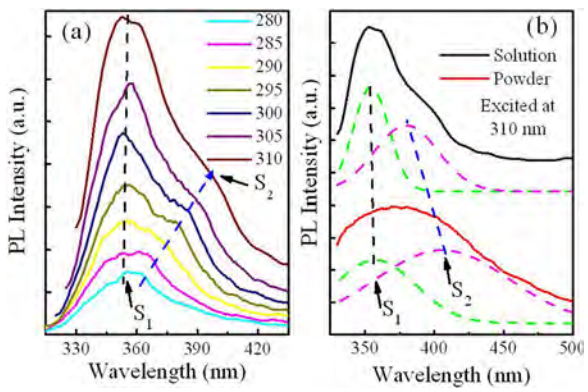

FIG. 1. (Color online) (a) PL spectra of the ultrathin cuboid SnO_2 NC suspension excited by the 280-310 nm lines of a Xe lamp. (b) PL spectra composed of tow subpeaks acquired from the suspension and dried powder excited by 310 nm.

a)Authors to whom correspondence should be addressed. Electronic addresses: hkxlwu@nju.edu.cn and paul.chu@cityu.edu.hk.

increasing NC size and meantime, the line-width increases as well. S_1 is close to the bandgap energy of ~3.65 eV (to be discussed in detail below), but S_2 has a lower energy. The observed PL may arise from band edge recombination as a result of relaxation from the forbidden dipole. To explore the mechanism, the NC suspension was dried in air at 100 °C for 5 h before taking another PL spectrum [Fig. 1(b)]. The PL spectrum is obviously broadened and composed of two subpeaks (S_1 and S_2 marked by green and magenta dash lines based on Gaussian fittings). Comparison to the PL spectrum of the colloidal suspension discloses that the effects of water on the optical emission are minimal. Moreover, the position of S_1 does not change, but S_2 downshifts and the line-width increases. This implies that the PL mechanism of the suspension and dried sample is similar and the surface structure induced by water is not the main factor. Since OVs in metal oxides play an important role in the electronic and phonon properties, the double peak should be associated with OVs on the NC surface.

The HR-TEM images acquired from the colloidal suspensions are depicted in Fig. 2(a). The NCs have a cuboid morphology with lateral dimensions of 4.0 nm, but the lengths are different (marked by dashed lines). The NCs have a rutile phase and grow mainly along the (001) direction.[15] A lateral face of the ultrathin cuboid NC with the 0.343 nm lattice fringe is the (110) crystalline plane. The selected-area electron diffraction (SAED) pattern in Fig. 1(b) shows three diffraction rings (from inner to outer) corresponding to the (110), (101), and (211) planes of rutile SnO_2. To confirm the existence of OVs, the Sn 3 d XPS spectrum obtained from the dried sample is displayed in Fig. 2(c). The binding energy of the Sn $3d_{5/2}$ peak at 487.1 eV indicates that the valence of Sn is 3.62,[17] suggesting the cuboid NCs are nonstoichiometric with a large number of OVs in the near surface. The Gaussian fitted cuboid NC length distribution shown in Fig. 2(d) shows that the NC lengths have a widely distribution from 6.0–13.5 nm and should be responsible for the dependence on excitation wavelength [Fig. 1(a)] induced by the NC size change. For a fixed OV content, increase in the NC length corresponds to a larger average distribution depth of OVs in the near surface due to the smaller surface-to-volume ratio. This is similar to the effects induced by annealing. The results and subsequent analyses suggest that the change in the OV depth distribution induced by the NC size change gives rise to the observed PL characteristics.

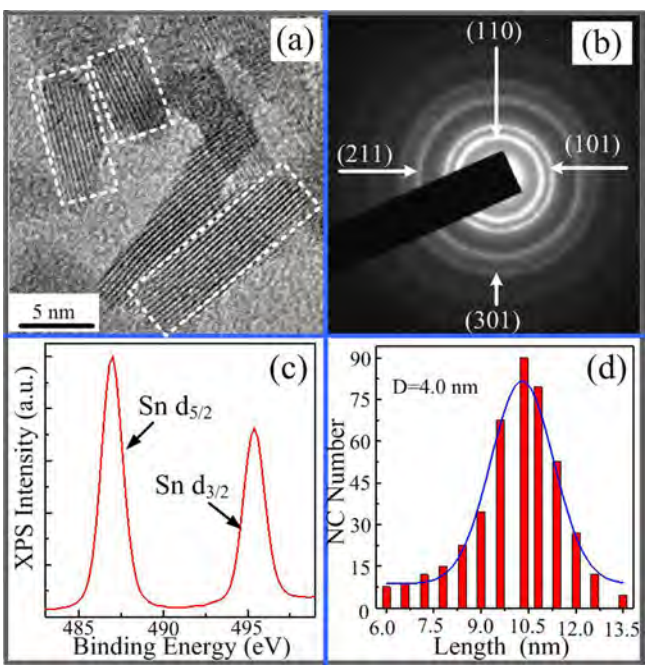

FIG. 2. (Color online) (a) Typical HR-TEM image of the SnO_2 NCs. (b) SAED pattern of the SnO_2 NCs. (c) Sn 3d XPS spectrum of the SnO_2 NCs. (d) Length distribution of the SnO_2 NCs with lateral width D of 4.0 nm.

Since the band gap of nanostructured materials can be different from that of the bulk counterparts, the ultraviolet/visible absorption spectrum obtained from the NC suspension is presented in Fig. 3. The absorption coefficient α is expressed as $\alpha(h\nu) \propto (h\nu - E_g)^{1/2}/h\nu$,[18] and plots of $[\alpha(h\nu)]^2$ vs $h\nu$ can be derived from the absorption data with the intercept of the tangent (marked by red line) corresponding approximately to the band gap energy of the direct band gap materials. As shown in Fig. 3, the average band gap of the cuboid NCs is ~3.65 eV which is slightly larger than that of bulk materials due to the quantum size effect. The two PL subpeaks have energies of 3.5 and 3.1 eV, which in the vicinity of the band gap of the cuboid NC. This implies that the observed PL should be associated with band edge recombination of the photo-excited carriers resulting from relaxation from the forbidden dipole due to the introduction of OVs. The Raman spectrum of the SnO_2 NC sample is displayed in the inset of Fig. 3. Besides the E_u longitudinal optical mode (f_1) at 355 cm^{-1} and A_{1g} mode (f_3) at 631 cm^{-1} which are related to the small size effect according to the Matossi force constant model,[19,20] an intense mode appears at 574 cm^{-1} (f_2) from the in-plane OVs (Ref. 21), but other types of OVs cannot be detected. Therefore, the double peak PL is inferred to stem from band edge recombination determined by the in-plane OVs which have different depth distributions in the near surface of the NC.

To theoretically elucidate the dependence of the PL peak on the OV depth distribution, a DFT study is conducted on several samples with different OV depth distributions. The calculation is based on the generalized gradient approximation of Perdew, Burke, and Ernzerholf using the CSATEP package with norm-conserving pseudopotential with default convergence tolerances of 1×10^{-5} eV for energy and

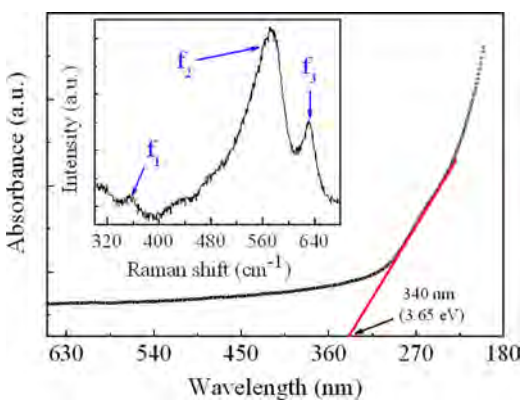

FIG. 3. (Color online) Ultraviolet/visible absorption spectrum acquired from the SnO_2 NCs. The inset shows the corresponding Raman spectrum.

0.03 eV/Å for maximum displacement.[22] The rutile SnO_2 (110) surface is modeled as a (1 × 1) supercell consisting of a six trilayer slab and vacuum with a thickness of five trilayers. The bottom two trilayers are fixed to mimic the bulk, and the in-plane oxygen atoms at different depths are removed. The density of states (DOSs) with the in-plane OV depth distributions at d = 0, 0.314, and 0.627 nm are calculated and shown in Fig. 4 and the result without OV is also presented for comparison. In the case of the less stable surface vacancy model, in which in-plane oxygen is absent from the stoichiometric surface, the highest occupied orbitals are significantly localized at the position of removed oxygen atom. Therefore, the DOSs at the valence-band maximum (VBM) can be modified by surface in-plane OV positions. According to the DOSs in Fig. 4 (left), the transition between the conductance band major peak near 3.56 eV (black arrow) and VBM at 0 eV corresponds to a 3.56 eV PL peak. Considering the under-estimation of the gap in the DFT calculation with the local density approximation (LDA) and generalized gradient approximation exchange-correlation function,[23,24] this is in good agreement with our experimental PL results. Here, it is interesting to note that addition of OV causes splitting of the DOS peak at the VBM (Fig. 4, right), which corresponds to the splitting of the PL peak observed experimentally and modified band gap. With increasing depths of OVs, splitting increases and the trend is consistent with experimental results.

It is known that both in-plane and bridging OVs may simultaneously exist in SnO_2 nanostructures. To reveal the different OV contributions, the DOSs of the SnO_2 nanostructure surfaces with different OV types are calculated and the corresponding results are presented in Fig. 5. Compared to the results without OV, the DOS (left) is significantly different in the presence of different OVs. The enlarged VBM regions with different kinds of OV situations are shown on the right side of Fig. 5. In the presence of in-plane OV, the DOS (green line) shows a clear double-peak structure, whereas the existence of a bridging OV effectively changes the DOS distribution into a single peak structure (red line). Considering the coexistence of in-plane and bridging OVs, the combined action not only causes splitting of the DOS (blue line) peak at the VBM but also modifies the intensities. The theoretical results indicate that the in-plane OV is responsible for the splitting of the DOS peak at the VBM. The bridging OVs may co-exist in the samples, but they are not the origin of the observed violet double-peak PL.

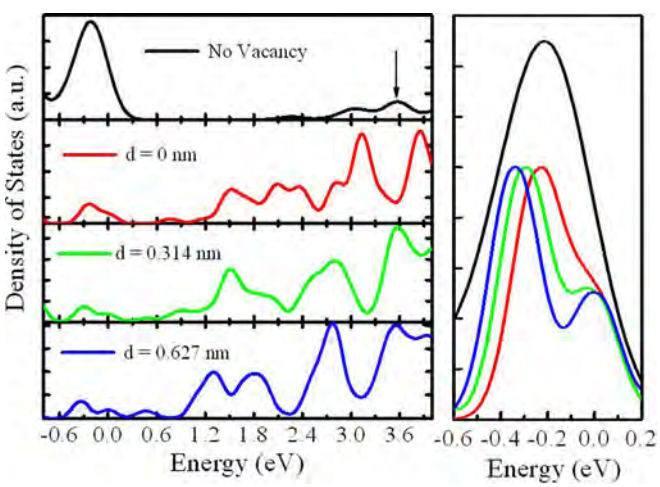

FIG. 4. (Color online) Left: DOSs of the cuboid NC surfaces with OV distribution depths at d = 0, 0.314, and 0.627 nm and no vacancy. Right: Enlarged VBM region. Splitting of the VBM due to addition of OV can be clearly seen and it leads to splitting of the PL peak observed experimentally.

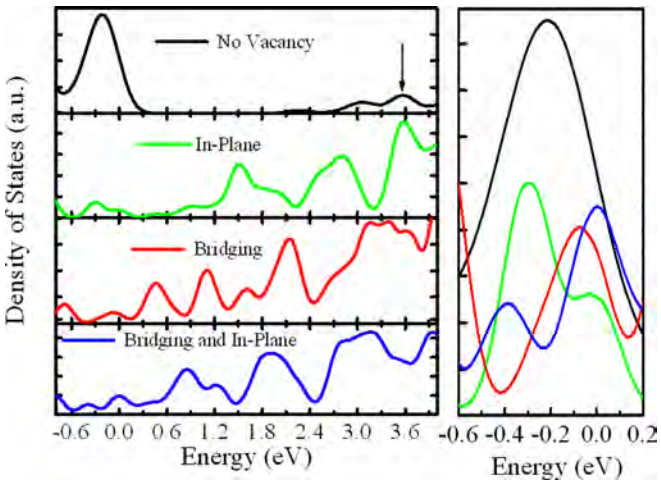

FIG. 5. (Color online) Left: DOSs of the cuboid NC surfaces with different OV types and no vacancy. Right: Enlarged VBM region. Splitting of the VBM due to addition of in-plane OV can be clearly observed. The bridging OVs do not cause the observed violet double-peak PL.

In summary, the PL spectra obtained from ultrathin cuboid SnO_2 NCs show a double peak in the violet region and the energy separation between the two subpeaks increases with NC size. It is related to changes in the in-plane OV depth distribution in the near surface of the NC. DFT calculation discloses that splitting of DOS at the VBM increases with OV depth distribution, thereby leading to band edge recombination. As a result, the PL peak splits and the two subpeaks shift oppositely, as verified by the experimental results.

This work was jointly supported by Grants (Nos. 2011CB922102 and 60976063) from the National Natural Science Foundation and Basic Research Programs of China. Partial support was also from PAPD, Postdoctoral Science Foundations of China and Jiangsu Province (Nos. 2011M500889 and 1102001B), and Hong Kong Research Grants Council (RGC) General Research Fund (GRF) No. CityU 112510.

[1]S. Brovelli, A. Chiodini, A. Lauria, F. Meinardi, and A. Paleari, Phys. Rev. B **73**, 073406 (2006).
[2]C. Killic and A. Zunger, Phys. Rev. Lett. **88**, 095501 (2002).
[3]H. T. Chen, S. J. Xiong, X. L. Wu, J. Zhu, J. C. Shen, and P. K. Chu, Nano Lett. **9**, 1926 (2009).
[4]Y. Idota, T. Kubota, A. Matsufuji, Y. Maekawa, and T. Miyasaka, Science **276**, 1395 (1997).
[5]R. Asahi, T. Morijawa, T. Ohwaki, K. Aoki, and Y. Taga, Science **293**, 269 (2001).
[6]G. Blattner, C. Klingshrin, and R. Helbig, Solid State Commun. **33**, 341 (1980).
[7]F. Arlinghaus, J. Phys. Chem. Solids **35**, 931 (1974).
[8]A. Kar, M. A. Stroscio, M. Dutta, J. Kumari, and M. Meyyappan, Appl. Phys. Lett. **94**, 101905 (2009).
[9]R. Chen, G. Z. Xing, J. Gao, Z. Zhang, T. Wu, and H. D. Sun, Appl. Phys. Lett. **95**, 061908 (2009).
[10]E. J. H. Lee, C. Ribeiro, T. R. Giraldi, E. Longo, and E. R. Leite, Appl. Phys. Lett. **84**, 1745 (2004).
[11]X. X. Xu, J. Zhuang, and X. Wang, J. Am. Chem. Soc. **130**, 12527 (2008).

[12]E. M. Wong and P. C. Searson, Appl. Phys. Lett. **74**, 2939 (1999).
[13]T. W. Kim, D. U. Lee, and Y. S. Yoon, J. Appl. Phys. **88**, 3759 (2000).
[14]M. A. Mäki-Jaskari and T. T. Rantal, Phys. Rev. B **65**, 245428 (2002).
[15]L. Z. Liu, X. X. Li, X. L. Wu, X. T. Chen, and P. K. Chu, Appl. Phys. Lett. **98**, 133102 (2011).
[16]L. Z. Liu, J. Wang, X. L. Wu, T. H. Li, and P. K. Chu, Opt. Lett. **35**, 4026 (2010).
[17]C. H. Liang, Y. Shimizu, T. Sasaki, and N. Koshizaki, J. Phys. Chem. B **107**, 9220 (2003).
[18]G. Mills, Z. G. Li, and D. Meisel, J. Phys. Chem. **92**, 822 (1988).
[19]Y. J. Chen, L. Nie, X. Y. Xue, Y. G. Wang, and T. H. Wang, Appl. Phys. Lett. **88**, 083105 (2006).
[20]J. Zou, C. Y. Xu, X. M. Liu, C. S. Wang, C. Y. Wang, Y. Hu, and Y. T. Qian, J. Appl. Phys. **75**, 1835 (1994).
[21]L. Z. Liu, X. L. Wu, F. Gao, J. C. Shen, T. H. Li, and P. K. Chu, Solid State Commun. **151**, 811 (2011).
[22]B. G. Pfrommer, M. Cote, S. G. Louie, and M. L. Cohen, J. Comput. Phys. **131**, 233 (1997).
[23]M. A. Maki-Jaskari and T. T. Rantala, Phy. Rev. B **64**, 075407 (2001).
[24]G. Cicero, A. Catellani, and G. Galli, Phy. Rev. Lett. **93**, 016102 (2004).